Biol. Cybern. 81, 25–37 (1999)

Biological Cybernetics

Early detection of upper airway obstructions by analysis of acoustical respiratory input impedance

S. Reisch[1,2], **H. Steltner**[2], **J. Timmer**[2], **C. Renotte**[3], **J. Guttmann**[1]

[1] Section of Experimental Anaesthesiology, Clinic of Anaesthesiology, University of Freiburg, Freiburg, Germany
[2] Center of Data Analysis and Model Building, University of Freiburg, Freiburg, Germany
[3] Faculté Polytechnique de Mons, Laboratoire d'Automatique, University of Mons, Mons, Belgium

Received: 23 July 1998 / Accepted in revised form: 26 January 1999

Abstract. Repetitive occurrence of partial or total upper airway obstruction characterizes several respiratory dysfunctions such as the obstructive sleep apnea syndrome (OSAS). In OSAS patients, pharyngeal collapses are linked to a decrease in upper airway muscle activity during sleep which causes decreased upper airway wall stiffness. Continuous positive airway pressure (CPAP) is recommended as the treatment of choice. Advancements in CPAP therapy require early detection of respiratory events in real time to adapt the level of the applied pressure to airway collapsibility. The forced oscillation technique (FOT) is a noninvasive method which reflects patients' airway patency by measuring respiratory impedance. The aim of this study was to evaluate by a mathematical model of the respiratory system if FOT can provide an early detection index of total or partial upper airway obstruction. Furthermore, the simulation should suggest which characteristic features are relevant for early apnea detection in measured clinical data. The respiratory system has been treated as a series of cylindrical segments. The oropharynx analog of the model allows simulation of upper airway collapse, mimicking the situation in patients with OSAS. We calculated the input impedance for different degrees of upper airway obstruction ranging from unobstructed airways to total occlusion. Furthermore, we simulated different upper airway wall compliances. We compared the simulation with real data. The results of the study suggest that FOT is a valuable tool for assessing the degree of upper airway obstruction in patients with OSAS. Especially, the phase angle of the impedance seems to be a potentially useful tool for early apnea detection by assessing the upper airway wall collapsibility.

Correspondence to: J. Timmer,
Center of Data Analysis and Model Building,
University of Freiburg, Eckerstr. 1,
D-79104 Freiburg, Germany
(e-mail: jeti@fdm.uni-freiburg.de,
Tel.: +49-761-203-7707, Fax: +49-761-2037700)

1 Introduction

Upper airway obstructions accompany several respiratory dysfunctions such as the obstructive sleep apnea syndrome (OSAS), which is characterized by recurring episodes of complete or partial pharyngeal obstruction during sleep. OSAS is associated with multiple episodes of sleep fragmentation and oxygen desaturation, with predominant symptoms of disruptive snoring and daytime sleepiness (Strohl and Redline 1996). The pathophysiology of OSAS has not been fully understood to date, although previous investigations have shown that contributory factors include (1) a sleep-induced decrease in upper airway dilator muscle activity, (2) an anatomically small pharyngeal airway, (3) relatively thick lateral pharyngeal walls, and (4) an increase in the total volume of parapharyngeal fat (Schwab et al. 1995; Mezzanotte et al. 1996; Schwartz et al. 1996). Furthermore, Kuna and Smickley (1997) have shown that activation of superior pharyngeal constrictors is not necessary to induce upper airway closure. They reported a decrease or complete cessation of superior pharyngeal constrictor activity during obstructive respiratory events.

Nowadays, continuous positive airway pressure (CPAP) is recommended as the treatment of choice achieving pharyngeal patency by pneumatic splinting of the collapsible segment. However, the increased work of breathing required to complete expiration against this pressure often results in a sensation of dyspnea (Kribbs et al. 1993). Furthermore, long-term effects on the lung due to the continuous overinflation have not been investigated yet. Therefore, the task arises to develop apnea-adapted CPAP devices which require methods for automatic early detection of respiratory events.

The forced oscillation technique (FOT) noninvasively measures respiratory impedance which reflects airway patency. Applying FOT, a pressure oscillation of small amplitude is superimposed on the breathing pattern of the patient, e.g. via a nasal mask. Respiratory impedance (Z) is derived from the pressure (P)–flow (V') re-

lationship of the FOT signal at the airway opening ($Z = P/V'$) with its components absolute value $|Z|$ and phase angle ϕ, $Z = |Z| \cdot e^{i\phi}; i^2 = -1$ (Michaelson et al. 1975; Làndsér et al. 1976). Since respiratory impedance is frequency dependent, various FOT methods have been developed in the past (DuBois et al. 1956; Michaelson et al. 1975; Làndsér et al. 1976; Cauberghs et al. 1984; Peslin and Fredberg 1986). The main differences between these methods are the frequencies applied and the way impedance is analyzed.

Initial studies suggested that FOT may be a valuable tool for the quantitative assessment of respiratory impedance in OSAS patients (Navajas et al. 1996; Reisch et al. 1996a; Rühle 1996; Farré et al. 1997). These studies showed in particular that the absolute value of impedance is related to the degree of airway obstruction. However, for early detection of OSAS, a signal is required which reflects upper airway muscle activity since a sleep-induced decrease in muscle activity precedes obstructive respiratory events. Such a decrease of muscle activity results in slackening of muscles surrounding the pharynx that usually dilate and stiffen the upper airway segments (Remmers et al. 1978). We therefore hypothesized that any change in upper airway muscle activity is equivalent to a change in upper airway wall stiffness and hence in compliance and should result in a change in the morphology of the phase angle $\phi(t)$ (Reisch et al. 1998).

The purpose of the present study was to obtain a qualitative and quantitative understanding of (1) the acoustical input impedance using a simplified mathematical model of the human respiratory system, (2) the input impedance for simulated upper airway obstructions of various degrees and (3) the input impedance for simulated sleep-induced decreases in upper airway dilator muscle activity by means of simulating different upper airway wall stiffness. The final goal was to demonstrate the potential value of FOT for early detection of upper airway obstructions by investigating the relationship between the stiffness of the pharyngeal wall and $\phi(t)$. This led to the derivation of characteristic features for early apnea detection in measured clinical data. We interpreted, finally, clinical FOT time series obtained from OSAS patients on the basis of the results obtained.

2 Theory

Performing an impedance measurement in parallel to CPAP therapy, the FOT signal is applied via a nasal mask (Rühle et al. 1997; Reisch et al. 1998). When the subject breathes through the nose with his mouth closed, this allows for the measurement of the respiratory impedance which comprises the following segments in series: (a) the nasal cavity, (b) the epipharynx, ranging from the choana/posterior nasal aperture down to the free end of the velum palatini, (c) the mesopharynx, ranging down to the free end of the epiglottis (frontally it is open to the oral cavity which usually is almost completely filled by the tongue in the case of relaxed quiet breathing during sleep), (d) parts of the hypopharynx (down to the aditus laryngis/laryngeal entrance), (e) the larynx, (f) the trachea and (g) the lung.

To investigate the influence of the wall stiffness of collapsing upper airways on the FOT signal, we used a model according to the electroacoustic theory. Figure 1 shows a scheme of the airway model. The respiratory system is modeled by four cylindrical segments, representing the nasopharynx analog NPA [corresponding to the above-mentioned segments (a) and (b)], the oropharynx analog OPA [segments (c) and (d)], the trachea analog TRA [segments (e) and (f)] and the lung analog LA [segment (g)]. The LA consists of a cylindrical segment whose volume changes during the respiratory cycle. The FOT source is located at the nasal airway opening and superimposes a flow rate $V'_{FOT}(t)$ on the respiratory flow. To simulate upper airway obstruction the OPA is divided into two subsegments, OPA I and OPA II with variable cross-sectional area (Fig. 2).

A uniform cylindrical segment (Fig. 1) having a plane wave passing through it, is analogous to a section of

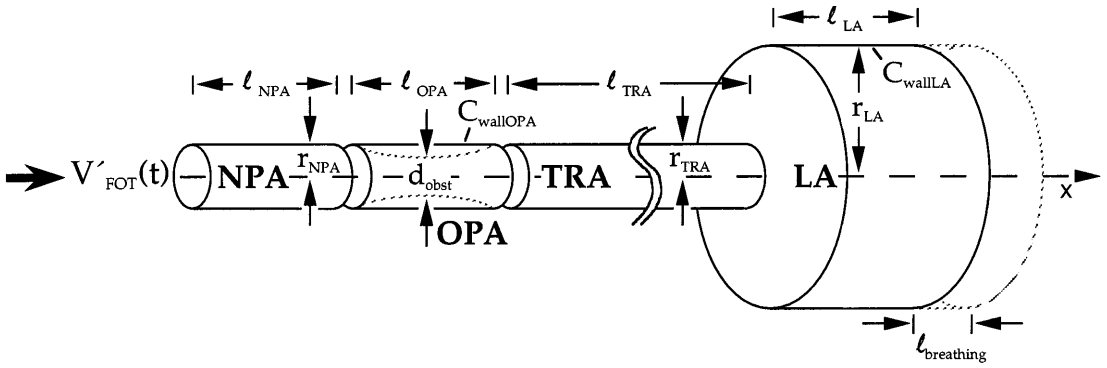

Fig. 1. Scheme of the airway model. $V'_{FOT}(t)$ Flow rate of the forced oscillation technique (FOT) signal at the airway opening, *NPA* nasopharynx analog; *OPA* oropharynx analog, *TRA* trachea analog; *LA* lung analog; ℓ_{NPA} length of the nasopharynx analog (4 cm); ℓ_{OPA} length of the oropharynx analog (4 cm); ℓ_{TRA} length of the trachea analog (12 cm); ℓ_{LA} length of the lung analog (9 cm); $\ell_{breathing}$ length variation of the lung analog due to tidal breathing (3.5 cm); r_{NPA} radius of the nasopharynx analog (0.9 cm); r_{TRA} radius of the trachea analog (0.9 cm); r_{LA} radius of the lung analog (7.5 cm); d_{obst} obstruction radius of the oropharynx analog; $C_{wallOPA}$ and C_{wallLA}, compliances of the oropharynx analog and of the lung analog wall, respectively

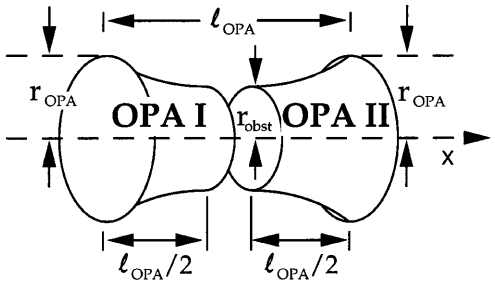

Fig. 2. Model of the upper airway obstruction assumed for the calculation. *OPA* oropharynx analog with the subsegments OPA I and OPA II; ℓ_{OPA} length of the oropharynx analog (4 cm); $\ell_{OPA}/2$ length of an OPA subsegment (2 cm); r_{OPA} radius of the unobstructed OPA (0.9 cm); r_{obst} obstruction radius of the oropharynx-analog

transmission line (Guelke and Bunn 1981). That is, the acoustical properties of a cylinder (resistance, inertance, conductance and compliance) can be described mathematically by differential equations for pressure and flow identical to those of an equivalent electrical circuit consisting of a resistance, an inductance, a conductance and a capacitance for electric potential and current. The transmission line theory was, therefore, used to derive the equations for the acoustical input impedance of the cylindrical segment. The theory is briefly described in Sect. 2.1.

Hypothesizing that changes in upper airway muscle activity are related to changes in upper airway wall stiffness (Reisch et al. 1996a, 1998), we decided to consider varying wall stiffness of the OPA to simulate a sleep-induced decrease in upper airway muscle activity. The theory of wave propagation in cylindrical segments with an elastic wall is described in Sects. 2.2 and 2.3.

The theory of determining input impedance for simulated partial and total upper airway obstruction is presented in Sect. 2.4.

2.1 Transmission line theory for isothermal and rigid tube walls

The theory of wave propagation in a tube with rigid walls is discussed in detail elsewhere (Dunn 1959; Benade 1968; Keefe 1983; Hudde 1988; Hudde and Slatky 1989). Briefly, consider a smooth cylindrical duct of radius a with rigid walls whose axis extends along the x-axis (Fig. 1). It is assumed that the FOT frequency is low enough to allow only a single mode which propagates energy over axial distances which are large compared to the tube diameter. Furthermore, laminar steady flow is considered for breathing. Thus, the respiratory system is thought to respond passively and linearly to forced oscillation. The frequency of the respiratory flow can be neglected because FOT frequencies normally used are far beyond the normal range of physiological respiratory frequencies and because the FOT amplitude is small compared with tidal breathing (Dorkin et al. 1982; Franken et al. 1986; Daviskas et al. 1990; Keyhami et al. 1995). The input/output relation of a cylindrical tube is given by the acoustic transmission line equations for lossy duct:

$$P_i = P_0 \cosh(\gamma\ell) + V_0' Z_0 \sinh(\gamma\ell) \tag{1a}$$

$$V_i' = P_0 \sinh(\gamma\ell)/(Z_0) + V_0' \cosh(\gamma\ell) \ . \tag{1b}$$

P_i and V_i' denote sound pressure and flow at the input, P_0 and V_0' the same at the output. ℓ is the length of the airway. The propagation coefficient γ and the characteristic wave impedance Z_0 are numerically evaluated according to the approximation given by Hudde and Slatky (1989).

The acoustical input impedance Z_i of the airway can be calculated according to Eqs. (1a) and (1b):

$$Z_i = \frac{Z_L \cosh(\gamma\ell) + Z_0 \sinh(\gamma\ell)}{(Z_L/Z_0)\sinh(\gamma\ell) + \cosh(\gamma\ell)} \ , \tag{2}$$

where Z_L denotes the impedance at the output of the airway.

2.2 Tube wall compliance

The wall compliance of a tube can be taken into account by multiplying both the propagation coefficient γ and the wave admittance $Y := \gamma Z_0$ by the factor (Hudde and Slatky 1989)

$$F_\omega = [1 + Y_\omega/(Y\gamma)]^{1/2} \ , \tag{3}$$

where Y_ω is the length-related wall admittance, and Y and γ are the unchanged values of wave admittance and propagation coefficient, respectively. For airways of the respiratory system the quantity Y_ω in Eq. (3) is given by

$$Y_\omega = \frac{1}{w + i\omega m + s/i\omega} \ , \tag{4}$$

where w denotes the specific (length-related) resistance of the airway, m the specific inertance, and s the specific stiffness (Hudde and Slatky 1989).

2.3 Model wall compliances

The onset of an obstructive respiratory event is characterized by a decrease in upper airway muscle activity, which is equivalent to a decrease of the specific stiffness s of the airway wall. Isono et al. (1997) have investigated the mechanical properties of the passive pharynx in normal subjects and OSAS patients. They applied general anesthesia, including muscle relaxation, to achieve complete paralysis of the pharyngeal muscles. In the absence of ventilation, they measured the mean cross-sectional areas A of the oropharynx as a function of airway pressures P_{aw} applied via a nasal mask ranging from 20 cm H_2O down to pharyngeal closing pressure. They fitted the pressure/area relationships by exponential functions $A = A_{max} - B\exp(-KP_{aw})$ with constants A_{max}, B and K for different patient groups. The specific

stiffness of a transmission line wall is given by $s = A(\mathrm{d}P_{\mathrm{aw}}/\mathrm{d}A)$ (Morse and Ingard 1968), where A denotes the cross-sectional area. Thus, the specific stiffness s can be calculated for a pharyngeal segment by

$$s = A/[K(A_{\max} - A)] \ . \tag{5}$$

The parameters determined by Isono et al. (1997) for the oropharynx for normal subjects are $A_{\max} = 3.0\,\mathrm{cm}^2$ and $K = 0.13\ (\mathrm{cm\,H_2O})^{-1}$ and for OSAS patients $A_{\max} = 2.1\ \mathrm{cm}^2$ and $K = 0.2\ (\mathrm{cm\,H_2O})^{-1}$. Taking these parameters and considering a nonobstructed oropharynx with a cross-sectional area A of 2.6–2.7 cm^2 for normals and A = 1.7–1.8 cm^2 for OSAS patients, the specific stiffness of the oropharynx varies between 5000 kg/(m s^2) and 7000 kg/(m s^2) for normal subjects and between 3000 kg/(m s^2) and 4000 kg/(m s^2) for OSAS patients in the described situation.

2.4 Simulation of upper airway obstruction

In this section, the theory to determine the input impedance of the model with partial and total upper airway obstruction is presented. To simulate upper airway obstruction, the oropharynx analog is divided into two subsegments: (a) OPA I, a segment with decreasing cross-sectional area $A = A_0/(1 + \lambda x)$ with the cross-sectional area $A_0 = A\ (x = 0)$ at the entrance of the segment, a positive constant λ, the x-axis being the symmetry axis of the segment; and (b) OPA II, a segment with increasing cross-sectional area $A = A_m[1 + \lambda(x - \ell_{\mathrm{OPA}}/2)]$, A_m being the cross-sectional area at the junction of OPA I and OPA II (Reisch et al. 1996b). The degree of obstruction $\mathrm{deg_{ob}} = 1 - A_m/A_0$ is related to the constant λ by

$$\lambda = [\mathrm{deg_{ob}}/(1 - \mathrm{deg_{ob}})] \cdot 2/\ell_{\mathrm{OPA}} \ .$$

Some area/distance functions of the OPA for different degrees of obstruction are shown in Fig. 3. This special form of variation of the cross-sectional area (Bessel tube) was chosen because it allows an analytical calculation of the input impedances as described in the following subsection and seems reasonable from a physiological point of view. Thus, the serial impedance $Z := Z_0\gamma$ and wave admittance Y of a transmission line can be expressed by

$$Z = i\omega L + R \tag{7a}$$

$$Y = i\omega C + G \ , \tag{7b}$$

where L is the serial inertia (per unit length of the transmission line), R the serial resistance, C the shunt compliance and G the shunt conductance (Benade 1968). In order to calculate the input impedances analytically, the four quantities have to fulfil the relations

$$R_{(x)} = \zeta_1 L_{(x)} \tag{8a}$$

and

$$G_{(x)} = \zeta_2 C_{(x)} \ , \tag{8b}$$

where ζ_1 and ζ_2 are constants.

Furthermore, $C \propto A$ and $L \propto 1/A$ holds in an ideal transmission line (Guelke and Bunn 1968).

2.4.1 Segment with decreasing cross-sectional area

The input impedance of a Bessel tube segment with decreasing cross-sectional area can be calculated by means of a linearly increasing inertia $L_{(x)}$ (Wagner 1947; Dunn 1950; Seskadri 1971)

$$L_{(x)} = L_0(1 + \lambda x) \ . \tag{9a}$$

Thus, the segment shunt compliance is decreasing in the opposite way:

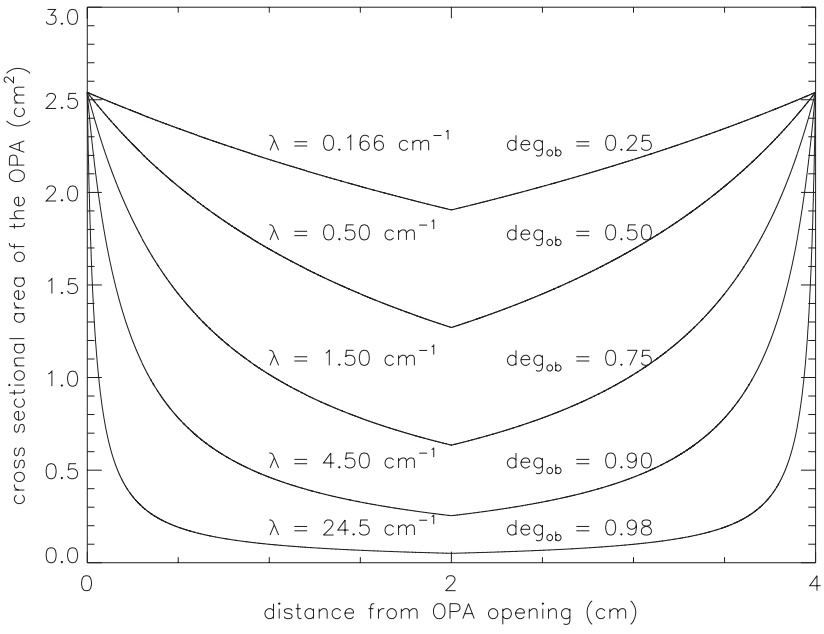

Fig. 3. Area distance functions of the oropharynx-analog for different degrees of obstruction $\mathrm{deg_{ob}}$. The oropharynx analog had a diameter of 1.8 cm in the unobstructed state and a length of 4 cm

$$C_{(x)} = C_0/(1+\lambda x) \ . \tag{9b}$$

L_0, C_0 and λ are constants. L_0 and C_0 denote the inertia and the compliance (per unit length of the transmission line) at the input of the segment, respectively. The wall of the segment is assumed to be rigid to allow for an analytical solution of the equations. Extending the procedure described in Sect. 2.2 would allow to include the specific resistance w, the specific inertance m and the specific stiffness s of the airway wall into the calculation of R, L, G and C of a Bessel tube, but Eqs. (8a)–(9b) would not be fulfilled anymore, disabling an analytic treatment. The theory is discussed in detail elsewhere (Wagner 1947; Seskadri 1971). Briefly, with ω denoting the radian frequency of the pressure oscillation, the following results are given for sound pressure ($P_{(x,t)}$) and flow ($V'_{(x,t)}$) within the segment:

$$P_{(x,t)} = (i\omega+\zeta_1)(1+\lambda x)\Big[c_1 H_1^{(1)}\Big(\frac{m}{\lambda}(1+\lambda x)\Big) + c_2 H_1^{(2)}\Big(\frac{m}{\lambda}(1+\lambda x)\Big)\Big]\mathrm{e}^{i\omega t} \tag{10}$$

$$V'_{(x,t)} = -\frac{m}{L_0}\Big[c_1 H_0^{(1)}\Big(\frac{m}{\lambda}(1+\lambda x)\Big) + c_2 H_0^{(2)}\Big(\frac{m}{\lambda}(1+\lambda x)\Big)\Big]\mathrm{e}^{i\omega t} \ . \tag{11}$$

$H_n^{(1)}$ and $H_n^{(2)}$ denote the Hankel functions of order n, and m is

$$m = \alpha - i\beta \ , \tag{12}$$

with

$$\alpha = \sqrt{\frac{L_0 C_0}{2}}\sqrt{(\omega^2-\zeta_1\zeta_2)+\sqrt{(\omega^2-\zeta_1\zeta_2)^2+\omega^2(\zeta_1+\zeta_2)^2}} \tag{13}$$

and

$$\beta = \sqrt{\frac{L_0 C_0}{2}}\sqrt{-(\omega^2-\zeta_1\zeta_2)+\sqrt{(\omega^2-\zeta_1\zeta_2)^2+\omega^2(\zeta_1+\zeta_2)^2}} \ . \tag{14}$$

The quantities c_1 and c_2 can be calculated as follows (Wagner 1947; Seskadri 1971):

1. $P_0\mathrm{e}^{i\omega t}$ denotes the sound pressure at the input ($x = 0$) of the airway segment. Then, using Eq. (10) we derive

$$P_0 = (i\omega+\zeta_1)\Big[c_1 H_1^{(1)}\Big(\frac{m}{\lambda}\Big) + c_2 H_1^{(2)}\Big(\frac{m}{\lambda}\Big)\Big] \ . \tag{15}$$

2. The impedance at the output of the segment ($x = \ell$) is assumed to be Z_L. The pressure at the output of the segment can then be expressed by

$$P_{(\ell)} = Z_\mathrm{L} V'_{(\ell)} \ . \tag{16}$$

Using Eqs. (10) and (11), we derive

$$\begin{aligned}(i\omega+\zeta_1)(1+\lambda\ell)&\Big[c_1 H_1^{(1)}\Big(\frac{m}{\lambda}(1+\lambda\ell)\Big) + c_2 H_1^{(2)}\Big(\frac{m}{\lambda}(1+\lambda\ell)\Big)\Big]\mathrm{e}^{i\omega t}\\ = Z_L\Big\{&-\frac{m}{L_0}\Big[c_1 H_0^{(1)}\Big(\frac{m}{\lambda}(1+\lambda\ell)\Big) + c_2 H_0^{(2)}\Big(\frac{m}{\lambda}(1+\lambda\ell)\Big)\Big]\mathrm{e}^{i\omega t}\Big\} \ .\end{aligned} \tag{17}$$

Equations (15) and (17) have to be solved in order to determine c_1 and c_2 (Wagner 1947; Seskadri 1971).

2.4.2 Segment with increasing cross-sectional area

The input impedance of a Bessel tube segment with increasing cross-sectional area can be calculated by means of a linearly increasing segment shunt compliance $C_{(x)}$ (Wagner 1947; Dunn 1950; Seskadri 1971) which can be given by

$$C_{(x)} = C_0(1+\lambda x) \tag{18a}$$

and a decreasing inertia

$$L_{(x)} = L_0/(1+\lambda x) \ . \tag{18b}$$

Again, the segment wall is assumed to be rigid to allow for an analytical solution of the equations. In analogy to Sect. 2.4.1, the following equations are obtained as results for sound pressure [$P_{(x,t)}$] and flow [$V'_{(x,t)}$] of the FOT oscillation in the segment:

$$P_{(x,t)} = -\frac{m}{C_0}\Big[c_1 H_0^{(1)}\Big(\frac{m}{\lambda}(1+\lambda x)\Big) + c_2 H_0^{(2)}\Big(\frac{m}{\lambda}(1+\lambda x)\Big)\Big]\mathrm{e}^{i\omega t} \tag{19}$$

$$V'_{(x,t)} = (i\omega+\zeta_2)(1+\lambda x)\Big[c_1 H_1^{(1)}\Big(\frac{m}{\lambda}(1+\lambda x)\Big) + c_2 H_1^{(2)}\Big(\frac{m}{\lambda}(1+\lambda x)\Big)\Big]\mathrm{e}^{i\omega t} \ . \tag{20}$$

The quantities ζ_1, ζ_2, c_1, c_2 and m can be obtained in the same way as described in Sect. 2.4.1.

2.5 Model parameters

The NPA, OPA and TRA had diameters of 1.8 cm and lengths of 4 cm, 4 cm, and 12 cm respectively, in the unobstructed status. The LA had a length of 9 cm and a diameter of 15 cm (functional residual capacity = 1.6 l). The length of the LA was varied between 9 cm and 12.5 cm to simulate tidal breathing (tidal volume = 0.63 l). A respiratory rate of 15 min^{-1} and an air temperature of 36 °C were assumed.

NPA and TRA were rigid tubes, whereas the LA had a compliant wall. Figure 4 shows the variation of specific stiffness s, specific resistance w and specific inertance m of the LA during three respiratory cycles. They were chosen according to the mean values for lungs determined by Hudde and Slatky (1989). Respiratory hysteresis was not taken into account.

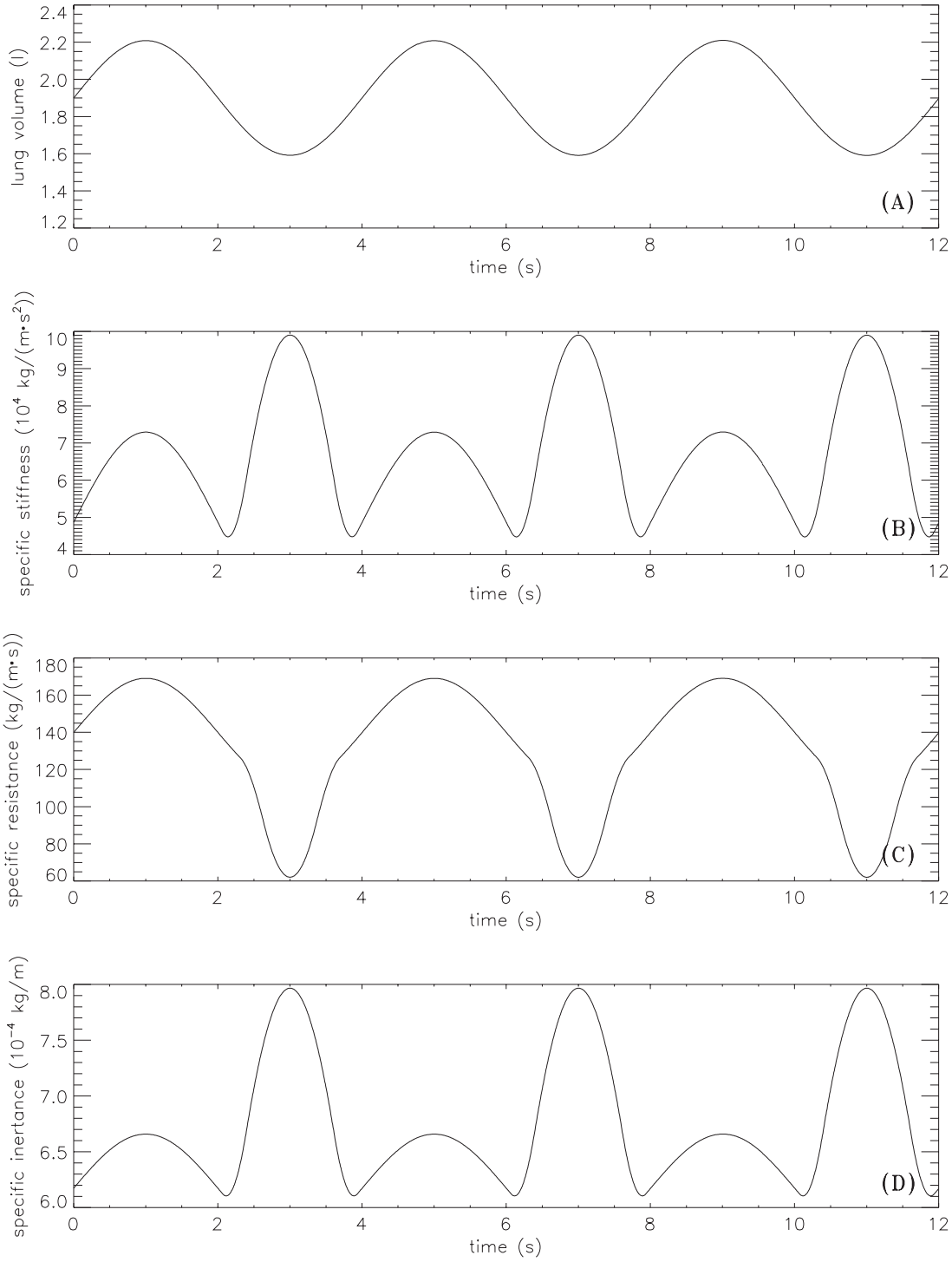

Fig. 4. Specific stiffness (**B**), specific resistance (**C**) and specific inertance (**D**) of the lung analog related to lung volume (**A**)

In the case of high muscle activity, the oropharyngeal walls are slightly less stiff than the tracheal walls. For decreased muscle activity, we assume that oropharyngeal walls are still stiffer than a completely paralyzed pharynx. Therefore, we chose $s_{OPA} = 70\,000\,\mathrm{kg/(m\,s^2)}$ for quiet breathing and $s_{OPA} = 30\,000\,\mathrm{kg/(m\,s^2)}$ as the minimum value to simulate collapsible upper airway walls. Hudde and Slatky (1989) have given values for s, m and w of different lung generations. As, to our knowledge, pharyngeal specific inertance and specific resistance have never been measured, we determined w and m of the OPA as functions of s on the basis of those values obtained by Hudde and Slatky (1989) by linear interpolation of the mean values (Fig. 5).

Ryan and Love (1996) have investigated changes of the pharyngeal cross-sectional areas between expiration (CSA_{ex}) and inspiration (CSA_{in}) by measuring $r_{CSA} = CSA_{ex}/CSA_{in}$ in normal subjects ($r_{CSA} = 1.1$)

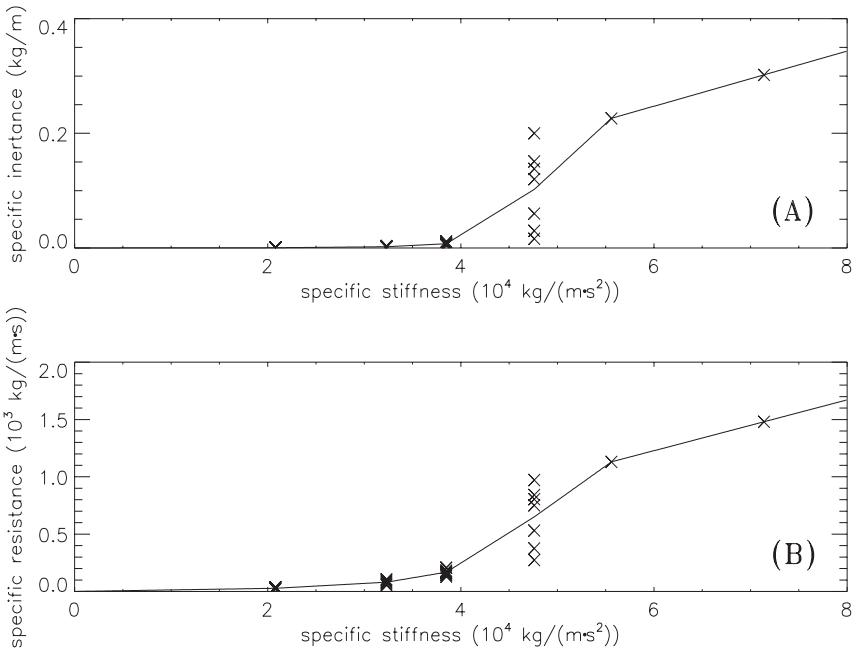

Fig. 5. Calculation of specific inertance (**A**) and specific resistance (**B**) on the basis of specific stiffness by linear interpolation of the mean of reference values for different lung generations. Each point in the figure represents a value tabulated by Hudde and Slatky (1989)

and OSAS patients ($r_{CSA} = 1.8$). This intra-breath variability of the OPA cross-sectional area was taken into account when simulating rigid upper airway walls only, using $r_{CSA} = 1.8$. It was not considered for compliant walls because an analytical treatment of a compliant Bessel tube is not feasible.

According to a clinical FOT setup (Rühle et al. 1997; Reisch et al. 1998), the input impedance of the model was calculated for a FOT frequency of 20 Hz.

2.6 Limitations of the model

Our mathematical model does not take into account all physiological and anatomical parameters. For example, neither the geometry of the bronchial tree, area/distance functions of human airways nor nonlinearities of the mechanical properties of airway walls nor clinical problems such as involuntary movements of the patient or swallowing are considered. Further, problems in daily routine such as mask leaks or an open mouth can only be simulated approximately. Any leak creates an additional impedance in parallel to the simulated system. As well, tidal volumes and breathing frequencies are constant throughout all simulations, not considering changes due to variations of the degree of obstruction.

Especially, the simulations rely heavily on the assumption of linearity. During normal breathing, turbulences of the gas flow are present in the nasal cavity, pharynx and trachea (Jaeger and Matthys 1970; Olson et al. 1970; Jebria et al. 1987; Leiter 1992). As a consequence, significant nonlinearities in the pressure/flow relationship of the FOT signal may occur when it interacts with the underlying respiratory flow. Louis and Isabey (1993) have investigated the validity of the assumption of linearity when superimposing FOT oscillations of frequency f on a steady turbulent flow of rate V' and found the condition $V' \leq 700\,\text{ml/s}$ for $f = 20\,\text{Hz}$ in unobstructed airways. Real peak flow rates at quiet breathing range from 125 ml/s to 200 ml/s. The aforementioned condition is not fulfilled when an obstruction occurs or during hyperventilation at the end of a respiratory event.

The impedance of the respiratory system is influenced by changes of both the cross-sectional areas and the lengths of all airway generations during a breathing cycle (Wiggs et al. 1990; Renotte et al. 1994). These intra-breath variabilities, together with turbulences, are reasons for the appearance of frequency doubled patterns in clinical $|Z(t)|$ and $\phi(t)$ time series (Peslin et al. 1992) compared to the respiratory rate.

Further, for an analytical calculation of the input impedance, the tube wall has to be rigid when simulating airway obstruction using a transmission line with a variable cross-sectional area. The specific resistance w of the tube wall, specific inertance m and specific stiffness s of such a segment can only be considered when performing a numerical simulation by finite elements.

The influence of heat transfer between the air and the tube walls during an oscillation as proposed by Keefe (1983) was evaluated. As the effect was negligible, we discarded this extension.

However, a comparison with empirical data shows that major physiological effects can be reproduced even with the simplified geometry of our model, only partially modeled intra-breath variabilities and assumptions of linearity.

3 Simulation studies

Three simulation studies were performed. In all simulations the parameters s, m and w of the LA wall varied with lung volume according to Fig. 4.

In simulation 1, input impedance was calculated for quiet spontaneous breathing with unobstructed OPA. s_{OPA} was 70 000 kg/(m s^2); the calculation of m_{OPA} and w_{OPA} was done according to Fig. 5. The cross-sectional area of the OPA was constant throughout the simulation ($r_{CSA} = 1$). At $t = 30$ s, the occurrence of a leak with a cross-sectional area of 2 mm^2 on the level of the airway opening was simulated. This leak should mimic a leaky nasal mask or an open mouth.

Upper airway obstruction was simulated by reducing the OPA radius r_{obst} (simulation 2). In contrast to simulation 1, the OPA wall is rigid even in the unobstructed state to allow for an analytical calculation of the input impedance. The input impedance was calculated for different degrees of obstruction ranging from unobstructed airways to total occlusion. Evolution of the degree of obstruction was adapted to the pathophysiological situation in OSAS patients. In the majority of the obstructive sleep apneas, upper airway collapses occur slowly and airway obstructions are abolished rapidly by an arousal. The simulation was performed with an elastic LA wall. r_{CSA} was 1.8 with an expiratory cross-sectional area of the OPA of 2.3 cm^2 in the unobstructed state (Ryan and Love 1996).

Finally, the specific stiffness of the OPA wall was varied (simulation 3). The specific stiffness was selected to range between 70 000 kg/(m s^2) for normal muscle activity and 30 000 kg/(m s^2) representing slackened muscles. The course of the specific stiffness of the OPA wall reflects pathophysiological situations; a slow decrease of upper airway wall stiffness characterizes the onset of respiratory events. The arousal which terminates respiratory events leads to a rapid increase of the specific wall stiffness. The OPA airway was open ($\deg_{ob} = 0$) as wall stiffness decreases preceding an obstruction and the cross-sectional area was kept constant throughout the simulation ($r_{CSA} = 1$).

3.1 Results

Figure 6 shows (A) the absolute value $|Z(t)|$ and (B) the phase angle $\phi(t)$ of the input impedance for (C) quiet spontaneous breathing calculated in simulation 1. $\phi(t)$ shows an oscillatory pattern of twice the respiratory frequency, ranging from -0.15π to -0.05π. When the leak occurs at $t = 30$ s $|Z(t)|$ is shifted towards lower values and $\phi(t)$ towards higher values.

The results of simulation 2 for both $|Z(t)|$ (A) and $\phi(t)$ (B) at different degrees of upper airway obstruction (C) are shown. Since the OPA wall is rigid the input impedance [$|Z(t)|$ and $\phi(t)$] for the unobstructed state ($t = 0$ s to 10 s) differs from the values obtained in simulation 1 (note the scaling of the y-axis). With increasing degree of obstruction, $|Z(t)|$ increases by more than a factor of 5 from unobstructed airways to the maximum degree of obstruction simulated. $\phi(t)$ shows a decrease in amplitude and a baseline shift towards lower values, also related to the degree of obstruction.

Figure 8 shows the input impedance of simulation 3 [(A) $|Z(t)|$ and (B) $\phi(t)$] for different specific stiffnesses of the OPA wall without upper airway obstruction. A minor increase of the baseline and decrease in the amplitude of $|Z(t)|$ can be observed. This change in the morphology of $|Z(t)|$, however, is negligible compared to that observed during an upper airway obstruction (Fig. 7, note the different scaling of the y-axis). For $\phi(t)$, a marked baseline shift towards higher values can be observed when reducing the specific stiffness of the OPA wall.

4 Application to measured data

We have frequently observed changes in the morphology of $\phi(t)$ measured in OSAS patients. Figure 9

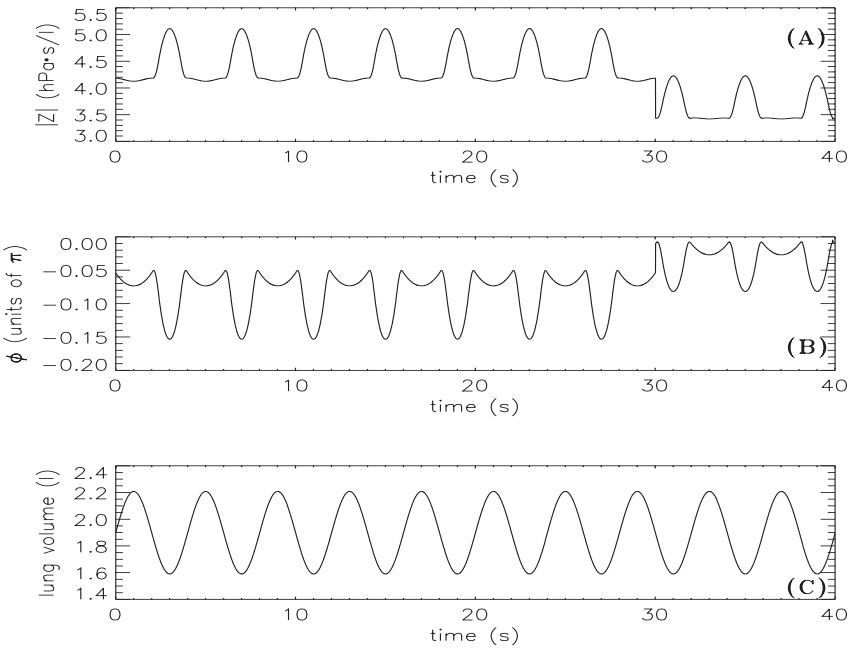

Fig. 6. A 40-s segment of **A** the absolute value $|Z(t)|$, **B** the phase angle $\phi(t)$ and **C** the lung volume for quiet breathing. The respiratory rate is 15 min^{-1}. At $t = 30$ s, a leak of cross-sectional area 2 mm^2 on the level of the NPA appears

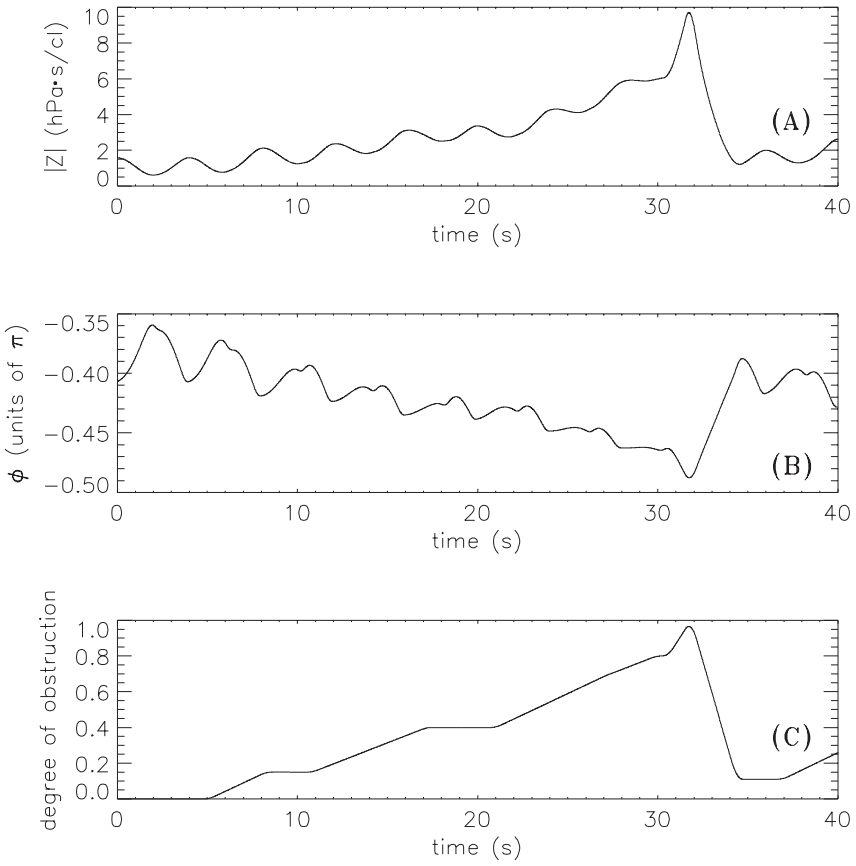

Fig. 7. A 40-s segment of **A** the absolute value $|Z(t)|$, **B** the phase angle $\phi(t)$ and **C** the degree of obstruction of the oropharynx analog. r_{CSA} of the OPA is 1.8. The respiratory rate is 15 min^{-1}

shows five typical segments of $|Z(t)|$ (thin line, lower tracing) and $\phi(t)$ (thick line, upper tracing). FOT was applied overnight within the scope of a polysomnography (Hospital Ambrock, Hagen, Germany). The FOT device which was connected in parallel to a CPAP device measures respiratory impedance at the nasal opening (Rühle et al. 1997; Reisch et al. 1998). Using such an integrated CPAP-FOT set-up, the value of the impedance depends on the individual CPAP set-up of the patient such as length of the CPAP tube or size of the nasal mask, which is part of the FOT reference impedance (Franetzki et al. 1979). Thus, the impedance is given in arbitrary units. The FOT device determines relative changes of airway impedance compared to a noncalibrated reference impedance. The analysis of data measured in OSAS patients is performed by evaluating changes in the morphology of the time series similar to those obtained in the simulations.

Figure 9A shows a 60-s period of quiet spontaneous breathing. During most of this period, the phase angle $\phi(t)$ shows an oscillation similar to the unobstructed state assuming rigid OPA walls during the first 10 s in simulation 2 (Fig. 7). The respiratory rate can be observed in $\phi(t)$. It is about 0.3 Hz. During some breathing cycles ($t = 39$ s to $t = 47$ s), $\phi(t)$ shows twice the frequency of the respiratory cycle which can be explained by simulation 1 (Fig. 6), i.e. an unobstructed OPA with compliant walls.

In Fig. 9B, a shift in baseline apparent in $\phi(t)$ can be observed with its onset at $t = 26$ s ($\Uparrow$) whereas the increase in $|Z(t)|$ is less pronounced. This situation can be interpreted based on simulation 3 (Fig. 8) in terms of a decreasing pharyngeal wall stiffness in preparation of an airway obstruction. An upper airway obstruction follows at $t = 42$ s ($\uparrow$) where a marked increase in $|Z(t)|$ is visible similar to simulation 2 (Fig. 7). Both time series show twice the frequency of the respiratory rate. This phenomenon can be explained by unrigid upper airway walls where both inspiration and expiration cause a decrease of the pharyngeal cross-sectional area.

In Fig. 9C, a first baseline shift in $\phi(t)$ starting at $t = 15$ s ($\Uparrow$) is observed, together with a slight increase in $|Z(t)|$, both in accordance with simulation 3 (Fig. 8). After $t = 28$ s an abrupt total occlusion occurs ($\uparrow$), reflected by a pronounced increase in $|Z(t)|$ together with a decrease in $\phi(t)$. This behavior during the obstruction can be explained by simulation 2 (Fig. 7), also confirming the results of a study on a mechanical model (Reisch et al. 1998). From $t = 39$ s ($\Uparrow$) to $t = 53$ s ($\uparrow$), a comparable event takes place.

In Fig. 9D, up to $t = 17$ s ($\Uparrow$), $\phi(t)$ follows the respiratory cycle in analogy to the unobstructed rigid OPA displayed in the first 10 s of simulation 2 in Fig. 7B. From $t = 17$ s until $t = 42$ s, $\phi(t)$ shows twice the respiratory rate. As for Fig. 7B, this can be explained by a decreased pharyngeal wall stiffness in preparation of the airway collapse. From $t = 42$ s until the obstruction,

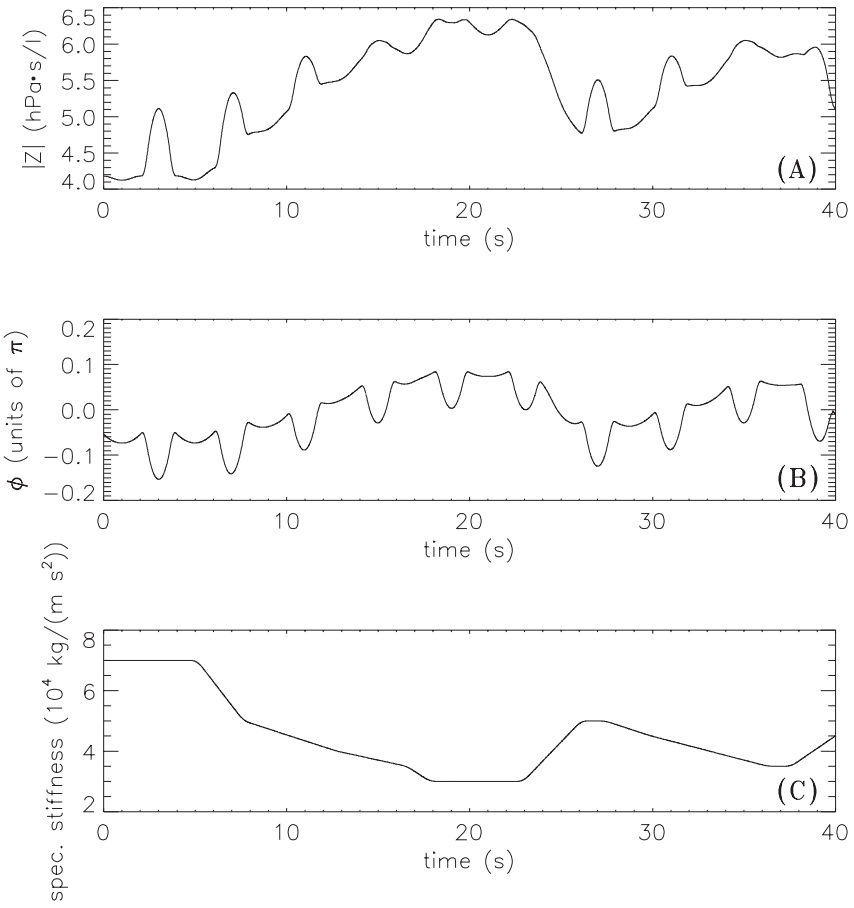

Fig. 8. A 40-s segment of **A** the absolute value $|Z(t)|$, **B** the phase angle $\phi(t)$ and **C** the specific stiffness of the OPA wall in the unobstructed state. The respiratory rate is 15 min^{-1}

beginning at $t = 50$ s (↑), the phase angle increases, in accordance with simulation 3 (Fig. 8B).

In Fig. 9E, three changes in the morphology of $\phi(t)$ can be observed. The data shown can be interpreted as follows: the upper airway muscle activity is reduced, which causes a frequency doubling and a baseline shift in $\phi(t)$ at $t = 9$ s (⇑). The upper airway wall, however, remains stiff enough to prevent an obstruction. The muscle tone increases again 20 s later, causing a second change in the morphology of $\phi(t)$ at $t = 29$ s (⇑). Concurrently, $\phi(t)$ changes back to a pattern as observed during quiet spontaneous breathing (compare Fig. 9A and beginning of Fig. 9D). The morphological change in $\phi(t)$ at $t = 50$ s (⇑) can be interpreted such that the upper airway wall stiffness decreases again, followed by a short upper airway obstruction which can be identified by the increase of $|Z(t)|$ at $t = 54$ s (↑). From $t = 50$ s on, $\phi(t)$ shows the frequency doubling reflecting decreased upper airway wall stiffness.

We have developed an algorithm to detect change points in $\phi(t)$ and investigated $\phi(t)$ data obtained in ten all-night FOT measurements of OSAS patients. The change points were classified retrospectively as potential onsets of respiratory events by five physicians. In total 3091 changes in the morphology of ϕ(t) were detected: 76.4% of the change points were classified as 'correct', 6.8% as 'false', and 16.8% as neither 'correct' or 'false'. 'Correct' means that the change points in $\phi(t)$ were linked to onsets of respiratory events. Change points classified as neither 'correct' or 'false' can be interpreted as decreases of the upper airway wall stiffness in preparation for upper airway collapse that finally do not result in an obstruction as in the data shown in Fig. 9E. Furthermore, the change points showed high correlation to the manual scoring of the staff physicians (Reisch et al. 1997).

5 Discussion

Although both the dynamics of upper airway obstruction are poorly understood and the presented theoretical model is a very simplified one only partly reflecting in vivo conditions, the model allows us to study main features considering the expected changes in $|Z(t)|$ and $\phi(t)$ of a FOT impedance measurement for (1) different degrees of upper airway obstructions, and (2) changes in the specific stiffness of the upper airway wall. The final goal of our study was to investigate by simulations if it is possible to use $\phi(t)$ as an early indicator for obstructive respiratory events by indicating changes in the collapsibility of the upper airways.

In summary, the data obtained by FOT for the model showed that the absolute value of the impedance $|Z(t)|$ is related to airway obstruction (Fig. 7). Thus, $|Z(t)|$ is a potential tool for detecting upper airway obstructions (Navajas et al. 1996; Rühle 1996; Farré et al. 1997). However, the detection is reliable only for degrees of

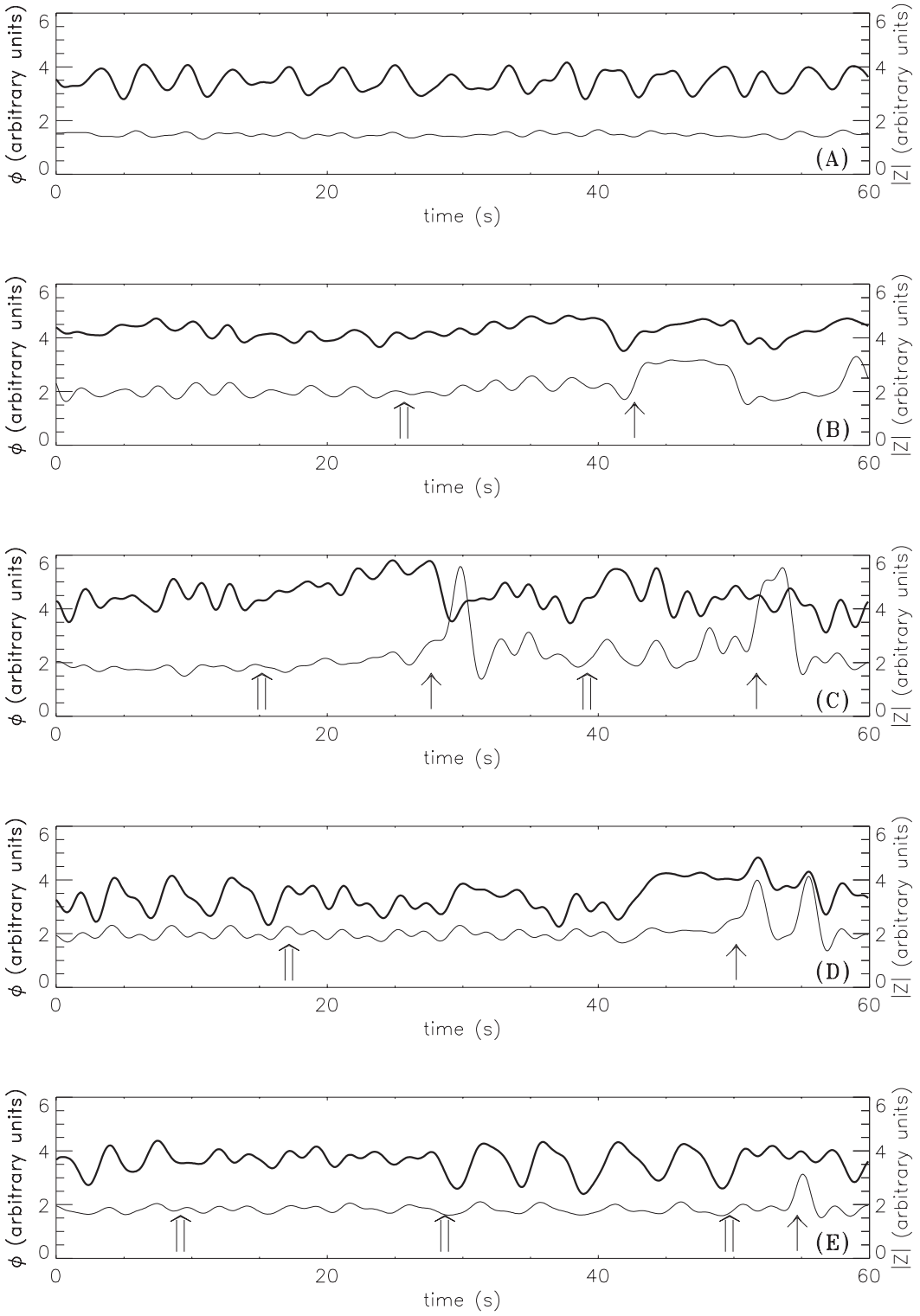

Fig. 9. Five 60-s segments of the absolute value $|Z(t)|$ (*thin line*, *lower tracing*) and phase angle $\phi(t)$ (*thick line*, *upper tracing*) of overnight FOT measurements from five patients. $|Z(t)|$ and $\phi(t)$ are low-pass filtered (Butterworth 6-poles, 0.5 Hz) and are given in arbitrary units of the D/A converter. **A** Quiet spontaneous breathing. **B**, **C** Baseline shifts apparent in $\phi(t)$ (⇑) followed by upper airway occlusions (↑). **D** A change in the morphology of the phase angle time curve (⇑) 30 s before $|Z(t)|$ increases (↑). **E** Changes in the morphology of $\phi(t)$ (⇑). The occlusion of the upper airway can be identified by the increase of $|Z(t)|$ (↑)

obstruction >0.8 (Reisch et al. 1998). For early detection, a signal is required which reflects the pathophysiological process that precedes the onset of a respiratory event. We hypothesized that the decreasing upper airway muscle activity which occurs in preparation for an obstructive respiratory event (Schwab et al. 1995; Mezzanotte et al. 1996; Schwartz et al. 1996; Kuna and Smickley 1997) causes a decrease of upper airway wall

stiffness, which enables the upper airways to collapse when the transmural pressure rises above a critical value (Farré et al. 1997). In other words, if we assume an increase in upper airway wall elasticity to characterize the onset of obstructive respiratory events, we expect the morphology of $\phi(t)$ to change significantly before an obstruction occurs (Fig. 8).

The proposed mathematical model is a simplification of the respiratory system not considering the complete set of physiological and anatomical parameters and assuming laminar flow conditions during quiet breathing. Nevertheless, a good accordance between simulated and measured input impedances is observed. Clinical data endorse several aspects of changes in the morphology of $|Z(t)|$ and $\phi(t)$ in agreement with simulated variations of upper airway geometry and elasticity. Postulated effects such as an increase in $\phi(t)$ in an early stage of an upper airway obstruction, a decrease in $\phi(t)$ when $|Z(t)|$ increases sharply, or changes in the morphology of $\phi(t)$ caused by a decrease of the upper airway wall stiffness can be observed in clinical data (Fig. 9). Furthermore, when the simulation is performed with realistic values of wall compliances or intra-breath variabilities of pharyngeal cross-sectional areas, the frequency doubled patterns in $|Z(t)|$ and $\phi(t)$ like those obtained in clinical impedance measurements can be observed.

The algorithm used in the measuring device of the clinical setup to calculate the absolute value and phase angle of the airway impedance makes use of several approximations; this could result in occasional masking of the effect of physiological changes on the phase angle signal. Furthermore, it could be speculated that a decreasing upper airway muscle activity also results in a slight decrease of pharyngeal cross-sectional area, too small to be visible in $|Z(t)|$; this would explain the decreasing amplitude of the $\phi(t)$ time series which can be observed together with the baseline shift in some of the examples in Fig. 9. Furthermore, not all patterns of the time series $|Z(t)|$ and $\phi(t)$ could be simulated due to the limitations of the mathematical model. Especially, the change to frequency doubled pattern at the onset of assumed decrease in upper airway wall stiffness could not be simulated with the model (Fig. 9D,E). This frequency doubling could be explained by a higher intra-breath variability of pharyngeal cross-sectional area due to slackened airway walls. Due to our demand for analytical treatment, this could not be integrated into our simulations. However, the results obtained yield a foundation for a qualitative interpretation of clinical data.

In patients, air leaks at the nasal mask cannot be completely avoided. The simulations show that the impedance measured by FOT is affected by the appearance of a leak which is placed in parallel with the patient's airway. The leak has a similar effect on the respiratory input impedance phase angle as upper airway wall compliance. As seen in Fig. 6, however, air leaks can be recognized by a disproportional decrease of $|Z(t)|$. An air leak caused by an open mouth has the same effect as a mask leak. However, clinical experience shows that the open mouth situation rarely occurs under CPAP therapy. The sealed mouth represents a constant upper airway shunt in parallel with the oropharynx, which plays a similar role to the individual configuration of the CPAP setup mentioned in section 4.

In conclusion, regarding all limitations of the mathematical model, this study suggests that FOT is a valuable tool for assessing the degree of upper airway obstruction in patients with OSAS. If applied to patients, the absolute value $|Z(t)|$ of the respiratory impedance enables us to determine the degree of upper airway obstruction. The data obtained show that the phase angle $\phi(t)$ can be useful to indicate decreased upper airway wall stiffness presumably related to muscle activity and, consequently, to predict upper airway obstruction. $\phi(t)$ is a promising tool for early detection of obstructive respiratory events.

Acknowledgements. We are grateful to Prof. Dr. K.-H. Rühle, Hagen, for valuable and stimulating discussions and the provision of the clinical data.

References

Benade AH (1968) On the propagation of sound waves in a cylindrical conduit. J Acoust Soc Am 44:616–623

Cauberghs M, Van de Woestijne KP (1984) Comparison of two forced oscillation techniques. Respiration 45:22–25

Daviskas E, Gonda I, Anderson SA (1990) Mathematical modeling of heat and water transport in human respiratory tract. J Appl Physiol 69:362–372

Dorkin HL, Jackson AC, Strieder DJ, Dawson SV (1982) Interaction of oscillatory and unidirectional flows in straight tubes and an airway cast. J Appl Physiol 52:1097–1105

DuBois A, Brody A, Lewis D, Burgess BF Jr (1956) Oscillation mechanics of lungs and chest in man. J Appl Physiol 8:587–595

Dunn HK (1959) The calculation of vowel resonances, and an electrical vocal tract. J Acoust Soc Am 22:740–753

Farré R, Peslin R, Rotger M, Navajas D (1997) Inspiratory dynamic obstruction detected by forced oscillation during CPAP – a model study. Am J Respir Crit Care Med 155:952–956

Franetzki M, Prestele K, Korn V (1979) A direct-display oscillation method for measurement of respiratory impedance. J Appl Physiol 46:956–965

Franken H, Clement J, Woestijne KP van de (1986) Superposition of constant and oscillatory flows in a rigid cylindrical tube: influence of entrance effects. IEEE Trans Biomed Eng 33:412–419

Franken H, Clement J, Caubergh, M, Woestijne KP van de (1981) Oscillating flow of a viscous compressible fluid through a rigid tube: a theoretical model. IEEE Trans Biomed Eng 28:416–420

Guelke RW, Bunn AE (1981) Transmission line theory applied to sound wave propagation in tubes with compliant walls. Acustica 48:101–106

Hudde H (1988) The propagation constant in lossy circular tubes near the cutoff frequencies of higher-order modes. J Acoust Soc Am 83:1311–1318

Hudde H, Slatky H (1989) The acoustical input impedance of excised human lungs – measurements and model matching. J Acoust Soc Am 86:475–492

Isono S, Remmers JE, Tanaka A, Sho Y, Sato J, Nishino T (1997) Anatomy of pharynx in patients with obstructive sleep apnea and in normal subjects. J Appl Physiol 82:1319–1326

Jaeger MJ, Matthys H (1970) The pressure flow characteristics of the human airways. In: Bouhuys A (ed) Airway dynamics, physiology and pharmacology, Thomas, Springfield, III, pp 21–32

Jebria BA, Tabka Z, Techoueyres P (1987) Steady pressure-flow relationship in a cast of upper and central human airways. Int J Biomed Comput 20:211–224

Keefe DH (1983) Acoustical wave propagation in cylindrical ducts: Transmission line parameter approximations for isothermal and nonisothermal boundary conditions. J Acoust Soc Am 75:58–62

Keyhani K, Scherer PW, Mozell MM (1995) Numerical simulation of airflow in the human nasal cavity. J Biomech Eng 117:429–441

Kribbs NB, Pack AI, Kline LR, Smith PL, Schwartz AR, Schubert NM, Redline S, Henry JN, Getsy JE, Dinges DF (1993) Objective measurement of pattern of nasal CPAP used by patients with obstructive sleep apnea. Am Rev Respir Dis 147:887–895

Kuna ST, Smickley JS (1997) Superior pharyngeal constrictor activation in obstructive sleep apnea. Am J Respir Crit Care Med 156:874–880

Làndsér FJ, Nagels J, Demedts M, Billiet L, Woestijne KP van de (1976) A new method to determine frequency characteristics of the respiratory system. J Appl Physiol 41:101–106

Leiter JC (1992) Analysis of pharyngeal resistance and genioglossal EMG activity using a model of orifice flow. J Appl Physiol 73:576–583

Louis B, Isabey D (1993) Interaction of oscillatory and steady turbulent flows in airway tubes during impedance measurement. J Appl Physiol 74:116–125

Mezzanotte WS, Tangel DJ, White DP (1996) Influence of sleep onset on upper airway muscle activity in apnea patients versus normal controls. Am J Respir Crit Care Med 153:475–480

Michaelson ED, Grassman ED, Peters WR (1975) Pulmonary mechanics by spectral analysis of forced random noise. J Clin Invest 56:1210–1230

Morse PM, Ingard KU (1968) Theoretical acoustics. New York McGraw-Hill, p 476

Navajas D, Farré R, Rotger M, Montserrat JM (1996) Assessment of airway obstruction by means of the forced oscillation technique during application of CPAP in patients with SAS (abstract). Am J Respir Crit Care Med 153:A772

Olson DE, Dart GA, Filey GF (1970) Pressure drop and fluid flow regime of air inspired into human lung. J Appl Physiol 28:482–494

Peslin R, Fredberg JJ (1986) Oscillation mechanics of the respiratory system. In: Handbook of Physiology, vol 3, part I. American Physiological Society, Bethesda, Md, pp 145–177

Peslin R, Ying Y, Gallina C, Duvivier C (1992) Within-breath variations of forced oscillation resistance in healthy subjects. Eur Respir J 5:86–92

Reisch S, Kulstrunk M, Timmer J, Schneider M, Rühle K-H, Geiger K, Guttmann J (1996a) Physikalisches Modell zur Simulation von Zeitverläufen der Atemwegsimpedanz bei obstruktiver Schlafapnoe. Biomed Tech 41[Supp l]:84-85

Reisch S, Renotte C, Timmer J, Honerkamp J, Geiger K, Guttmann J (1996b) Theoretische Evaluierung der Resisto-Oszillometrie bei obstruktiver Schlafapnoe. Biomed Tech 41[Supp l]:108–109

Reisch S, Timmer J, Rühle K-H, Geiger K, Guttmann J (1997) Detektion von obstruktiven Schlafapnoen durch statistische Analyse der Phasenwinkelveränderungen der Atemwegsimpedanz. Biomed Tech 42[Supp l]:295–296

Reisch S, Schneider M, Timmer J, Geiger K, Guttmann J (1998) Evaluation of forced oscillation technique for early detection of airway obstruction in OSAS patients: a model study. Technol Health Care 6:245–257

Remmers JE, De Groot WJ, Sauerland EK, Anch AM (1978) Pathogenesis of upper airway occlusion during sleep. J Appl Physiol 44:931–938

Renotte C, Remy M, Saucez P (1998) Dynamic model of airway pressure drop. Med Biol Eng Comput 36:101–106

Rühle K-H (1996) Oszillatorische Impedanz bei schlafbezogenen Atemregulationsstörungen. Thieme, Stuttgart

Rühle K-H, Schlenker E, Randerath W (1997) Upper airway resistance syndrome. Respiration 64[Suppl 1]:29–34

Ryan CF, Love LL (1996) Mechanical properties of the velopharynx in obese patients with obstructive sleep apnea. Am J Respir Crit Care Med 154:806–812

Schwab RJ, Gupta KB, Gefter WB, Metzger LJ, Hoffmann EA, Pack AI (1995) Upper airway and soft tissue anatomy in normal subjects and patients with sleep-disordered breathing. Am J Respir Crit Care Med 152:1673–1689

Schwartz AR, Eisele DW, Hari A, Testerman R, Erickson D, Smith PL (1996) Electrical stimulation of the lingual musculature in obstructive sleep apnea. J Appl Physiol 81:643–652

Seskadri SR (1971) Fundamentals of transmission lines and electromagnetic fields. Addison Wesley, New York

Strohl KP, Redline S (1996) Recognition of obstructive sleep apnea. Am J Respir Crit Care Med 154:279–289

Teschler H, Berthon-Jones M, Thompson AB, Henkel A, Henry J, Konietzko N (1996) Automated continuous positive airway pressure titration for obstructive sleep apnea syndrome. Am J Respir Crit Care Med 154:734–740

Wagner KW (1947) Einführungen in die Lehre von den Schwingungen und Wellen. Dieterich'sche Verlagsbuchhandlungen, Wiesbaden

Wiggs BR, Moreno R, Hogg JC, Hilliam C, Pare PD (1990) A model of the mechanics of airway narrowing. J Appl Physiol 69:849–860